


RESEARCH ARTICLE

Inter-annual variation of tropical cyclones simulated by GEOS-5 AGCM with modified convection scheme

Eunkyo Seo¹  | Myong-In Lee¹ | Dongmin Kim^{1,2,3} | Young-Kwon Lim^{4,5} |
Siegfried D. Schubert⁴ | Kyu-Myong Kim⁴

¹School of Urban and Environmental Engineering,
Ulsan National Institute of Science and
Technology, Ulsan, South Korea

²Cooperative Institute for Marine and Atmospheric
Studies, University of Miami, Coral Gables,
Florida

³Atlantic Oceanographic and Meteorological
Laboratory, Physical Oceanography Division,
NOAA, Miami, Florida

⁴Global Modeling and Assimilation Office, NASA
Goddard Space Flight Center, Greenbelt, Maryland

⁵Goddard Earth Sciences Technology and
Research, NASA Goddard Space Flight Center,
I. M. Systems Group, Rockville, Maryland

Correspondence

Myong-In Lee, School of Urban and
Environmental Engineering, Ulsan National
Institute of Science and Technology, 50 UNIST-
gil, Ulsu-gun, Ulsan 689-798, South Korea.
Email: milee@unist.ac.kr

Funding information

Korea Meteorological Administration Research
and Development Program, Grant/Award Number:
KMI2018-03110

The Goddard Earth Observing System version 5 (GEOS-5) global climate model with a 50-km horizontal resolution is forced by observed sea surface temperature (SST) to examine the fidelity of the seasonal-mean and inter-annual variation of tropical cyclones (TCs) in the western North Pacific (WNP) and the North Atlantic (NATL). The standard Relaxed Arakawa Schubert (RAS) deep convection scheme is modified to improve the representation of TCs, where the scheme implements a stochastic limit of the cumulus entrainment rate. The modification drives mid- and upper-tropospheric cooling and low- to mid-tropospheric drying in the background state, which tends to increase atmospheric instability. This enables the model to increase convective variability on an intra-seasonal timescale and improve the simulation of intense storms.

Five-member ensemble runs with the modified RAS scheme for 12 years (1998–2009) exhibit realistic spatial distributions in the climatological-mean TC development area and their pathways over WNP and NATL. The GCM is able to reproduce the inter-annual variation of accumulated cyclone energy (ACE) by prescribing yearly varying observed SST even though the individual TC intensity is still underpredicted. A sensitivity of TC activity to El Niño–Southern Oscillation (ENSO) phase is also reproduced realistically over WNP in terms of the spatial pattern changes in the main development region and TC pathways. However, the model exhibits a notable deficiency in NATL in reproducing the observed inter-annual variation of TC activity and the sensitivity to the ENSO.

KEYWORDS

accumulated cyclone energy, convection scheme, global climate model, inter-annual variation, tropical cyclone

1 | INTRODUCTION

Increasing computer resource enables us to simulate tropical cyclones (TCs) using global climate models (GCMs) and improve our understanding on their development mechanisms and spatiotemporal variability. Manabe *et al.* (1970) and Bengtsson *et al.* (1982) performed low-resolution model experiments in coarse horizontal resolution, which simulated a TC-like low-level disturbance using a GCM. With an increase of spatial resolution, GCMs have realistically

resolved the spatial distribution of main TC development regions and pathways as well as their inter-annual changes (Vitart *et al.*, 1997; Bengtsson *et al.*, 2007; LaRow *et al.*, 2008; Zhao *et al.*, 2009; Chen and Lin, 2011). Zhao *et al.* (2009) tested the 50-km horizontal resolution run to show the realistic secular trend of TC number over the whole TC development basins. They also found that the inter-annual variation of TC number with four-member ensemble simulations was significantly correlated with the observed in WNP and NATL when the model was driven by observed SST.

Other studies also addressed that a major leading tropical SST mode, ENSO, had the significant impact on the simulated TC variability in inter-annual timescale, for example, the genesis number, intensity, and geographical distribution of TCs over WNP (Chan, 1985; Matsuura *et al.*, 1999; Vitart and Anderson, 2001; Mei *et al.*, 2015; Han *et al.*, 2016; Zhang *et al.*, 2016) and NATL (Wang *et al.*, 2014; Mei *et al.*, 2014), respectively.

In the high-resolution GCM intercomparison studies conducted by the US CLIVAR Hurricane Working Group (<http://www.usclivar.org/working-groups/hurricane>) (Shaevitz *et al.*, 2014; Wang *et al.*, 2014; Walsh *et al.*, 2015; Han *et al.*, 2016), Shaevitz *et al.* (2014) showed that even though a few models were able to reproduce realistic TC activities with high correlation with observations, there was a wide spread in TC intensity and genesis number among the simulations by tested 12 GCMs. Specifically, most of the models exhibited a severe underprediction in TC intensity. The inter-model differences appear to be associated largely with the differences in horizontal resolution and model physics parameterization, but what drives these differences are not clearly understood and remain to be answered in future studies.

Model resolution has been regarded as one of the critical contributors to improve the simulated frequency of TCs (Walsh *et al.*, 2007; Walsh *et al.*, 2013; Murakami *et al.*, 2015). Successively increasing the resolution in a GCM shifted the probability distribution function (PDF) distribution of low-level absolute vorticity towards a stronger magnitude, which tended to improve the TC genesis (Strachan *et al.*, 2013). Overall TC intensity was intensified with more realistic relationship between the maximum 10-m wind speed and the minimum sea level pressure (SLP) in higher resolution experiments with a single model (Roberts *et al.*, 2015). A 25-km resolution run of the GEOS-5 GCM was able to simulate intensive TCs as strong as 65 m/s in the maximum surface wind speed (Lim *et al.*, 2015). The model was further tested in 7 and 14-km resolution to demonstrate the ability to simulate the category 5 TCs based on the Saffir-Simpson hurricane intensity scale (Saffir, 1977) as well as TC vertical structure with a distinguishable eyewall (Putman and Suarez, 2011), although such a large computing resource would not be available for routine forecasts in the current state.

There have been other studies attempting to improve the TC simulation through adjusting convective parameterization scheme in global models (Slingo *et al.*, 1994; Smith, 2000; Sanderson *et al.*, 2008; Zhao *et al.*, 2012; Lim *et al.*, 2015). Several studies controlled the scheme by applying a minimum entrainment threshold for convective plumes (Tokioaka *et al.*, 1988; Lee *et al.*, 2003; Held *et al.*, 2007; Kang *et al.*, 2008; Lin *et al.*, 2008). Using the threshold, Lim *et al.* (2015) simulated more realistic spatial feature of TCs and their intensity over NATL for several years at

25-km horizontal resolution. That study found a strong sensitivity of the simulated TCs to the modified convection scheme, where it tended to suppress the parameterized convection and increase ambient atmospheric instability, leading to stronger convection once triggered. The simulation result from Lim *et al.* (2015) suggests that even at 25-km horizontal resolution, improvement in the TC simulation should not be a direct consequence of the resolution increase. Considering that different GCMs in relatively coarse resolution of 50 km or lower such as in LaRow *et al.* (2008) and Zhao *et al.* (2009) simulated realistic inter-annual variation of TC frequency, it is worthy of more in-depth studies how the moist physics parameterizations, specifically the modification of the cumulus convection scheme within model, can influence on the TC simulation as well as on the background state. The model sensitivity runs using a single model will highlight the important role of the convection scheme among the various physics parameterizations implemented in the model and help understand the inter-model differences appearing in the previous GCM intercomparison studies.

This study using the GEOS-5 model at 50-km horizontal resolution is basically an extension of Lim *et al.* (2015). Using an identical model, the previous study demonstrated substantial improvement in the TC simulation in terms of their development region and pathways in NATL, although the impacts from the modified convection scheme on model background state and the TC simulations remained for a further study. This study examines to what degree the modification in the convection scheme could achieve improvements in the TC simulation, yet preserving realistic time-mean state, based on long-term ensemble model integration that help address the impacts from inter-annually varying SST on the TC variability. The comparison of this study with Lim *et al.* (2015) helps address if the modification is also positive even at 50-km horizontal resolution, not only in NATL but also in WNP. The study further investigates if there are any negative impacts on the model background state. This study presents here; (a) the impacts driven by the modification of convective parameterization on the time-mean state and subseasonal variability, and (b) the seasonal to inter-annual variability of TC. The GEOS-5 with modified convective parameterization is utilized for five-member ensemble simulations over 12 years (1998–2009).

In section 2, we introduce the GEOS-5 experimental design with the specific parameterization methodology for how to modify the deep convective scheme. In addition, the description of observational data sets and an algorithm used to detecting the simulated TCs are described in the section. Section 3 presents the results from the mean climatology of atmospheric backgrounds, and TC climatology, inter-annual variation and sensitivity to ENSO. Finally, summary and conclusion are given in section 4.

2 | MODEL EXPERIMENT AND DATA

2.1 | Model experiments

This study uses the GEOS-5 model developed by NASA Global Modeling and Assimilation Office (Suarez *et al.*, 2008; Molod *et al.*, 2012). Model experiments are conducted with a version of 50-km horizontal resolution and 72 hybrid-sigma vertical levels extending to 0.01 hPa. The model is integrated from May 15 to December 1 each year for the entire period of 12 years (1998–2009) with prescribed weekly SST forcing (Reynolds *et al.*, 2002) from Hadley Centre Sea Ice and Sea Surface Temperature observation data (HadISST; Rayner *et al.*, 2003).

The model is driven with a modified version of the RAS deep convection scheme (Moorthi and Suarez, 1992). Major modifications from the original version include the selection of convection starting level at the top of the planetary boundary layer. The convective adjustment timescale for the convective plumes increases linearly from 30 min to 12 hr at the increase of the vertical depth of plumes. An important modification is the implementation of the minimum entrainment rate (λ_0) threshold for convective plumes, which is defined as $\lambda_0 = \alpha/D_m$, where $\alpha = 0.2$ is a fixed parameter and D_m is the state-dependent parameter representing the depth of the sub-cloud layer (Tokiona *et al.*, 1988). Lim *et al.* (2015) selected D_m randomly with a power law probability distribution as

$$D_m = \beta \times x^n, \quad 0 \leq x \leq 1, \quad (1)$$

where β is an allowable maximum plume radius (Simpson and Wiggert, 1969), x is a random number between 0 and 1 for each integration time step and $n = -1/2$. Based on the initial observational study, β is objectively determined by the spatial resolution of the simulation (Bacmeister and Stephens, 2011). For the 50-km horizontal resolution run in this study, β is set to 500. The specification of λ_0 acts not only as a convection trigger ($\lambda \geq \lambda_0$, λ is the simulated entrainment rate), but also affects the closure assumption where the cloud work function for each plume is multiplied by a factor:

$$\gamma = [\lambda/\lambda_0]^2, \quad 0 \leq \gamma \leq 1. \quad (2)$$

To examine the simulation sensitivity to the stochastic limit of the entrainment for convective plumes, we conduct the runs with and without the modification for 12 years research period, which is referred to as “MOD” and “STD,” respectively. Five ensemble runs for the MOD configuration are produced by using different initial states for atmosphere and land, which are selected randomly from existing long-term simulations. For a comparison, this study also conducts one-member STD experiment with unmodified cumulus scheme. To be discussed in Section 3b, the original version of GEOS-5 (STD) tends to underestimate the TC number significantly. Although the

STD run consists of only a single realization the results are not expected to be different significantly from the case of multiple realizations.

2.2 | Validation data

Simulated precipitation are validated with the Tropical Rainfall Measuring Mission (TRMM; Huffman *et al.*, 2007) product 3B42 version 7 observation data, which are 3-hourly data in 25-km horizontal resolution. The Modern-Era Retrospective analysis for Research and Application (MERRA) atmospheric reanalysis data set (Rienecker *et al.*, 2011) is also used for the validation of atmospheric temperature, wind, and humidity, which has a $1/2^\circ$ lat. \times $2/3^\circ$ lon. horizontal resolution for selected vertical levels.

For the verification of TCs, this study uses the best track data from the International Best Track Archive for Climate Stewardship (IBTrACS, v03r03 released in July 2011; Knapp *et al.*, 2010) released by the NOAA National Climate Data Center. The 6-hourly data provide the centre location of TCs, SLP, and 10-m sustained wind speed.

2.3 | Detection method of TC

This study uses the TC detection and tracking algorithm, following the basin-dependent threshold method developed by Camargo and Zebiak (2002). The thresholds cover the critical values for dynamic and thermodynamic variables characterizing major features of TCs, including relative vorticity at 850 hPa (ζ_{850}), wind speed at 10 m (V_{10}) above the surface, and the vertically integrated temperature anomalies (T_{sum}) for 200, 500, and 700 hPa levels. The algorithm first calculates standard deviations for those variables using 6-hourly data for the entire time and spatial domain and for each basin. Then the algorithm searches the domain by moving a $5 \times 5^\circ$ box at 6-hr interval data and detects TCs when all three variables at any instant time and location exceed 2 (WNP) and 1.5 (NATL) times of their standard deviation values simultaneously. Besides, the detected TC needs to sustain longer than 2 days. Once any specific TC is detected, then the tracking algorithm reconstructs the entire path by tracking the vorticity centre back and forth when it meets the 850hPa vorticity threshold of $2.0 \times 10^{-4} \text{ s}^{-1}$ or higher. The same TC tracking and detection algorithm is applied to both STD and MOD runs.

2.4 | Representative TC features

In previous studies, they suggested indicators to represent the actual threat of TC. For instance, Emanuel (2005) introduced a power dissipation index (PDI) and Camargo and Sobel (2005) suggested accumulated cyclone energy (ACE) where both of terms are based on the maximum near surface wind speed for the TC lifetime. In this study, we adopt the concept of ACE. The individual TC intensity is defined,

$$\text{Individual intensity} = \frac{1}{N_y} \sum_{n=1}^{N_y} \frac{V_{n,y}^2}{\Delta t_{n,y}}, \quad (3)$$

where $V_{n,y}^2$ is the square of the TC's maximum sustained wind speed at 10 m altitude (the unit is m^2/s^2), accumulated over all 6 hr intervals for n th TC at y year, and $\Delta t_{n,y}$ is an individual TC lifetime (the unit is day). N_y is the total number of TC developed at the year. The other considerable term to indicate the sustained period of total developed TCs, a duration, is defined as the multiplication of the individual TC lifetime and the genesis number of TC at the year,

$$\text{Duration} = N_y \Delta t_{n,y}. \quad (4)$$

Multiplying the individual TC intensity and the duration yields the ACE and its unit is m^2/s^2 .

3 | RESULTS

3.1 | Mean climatology

We first examine the impacts of modified convection scheme on the simulated basic climate structure. Figure 1 compares the June–October mean precipitation patterns averaged for 12 years between the TRMM observation and the

two model simulations with the standard deep convection scheme (STD) and the modified scheme (MOD), respectively. Regardless of the differences in convection scheme, both simulations (Figure 1b,c) in general show realistic precipitation patterns. Both simulations also show similar bias patterns, such as stronger Intertropical Convergence Zone (ITCZ) in the central and eastern Pacific and larger rainfall in the Northwest Pacific, and the double ITCZs-like pattern in the Indo-Pacific region with a dry zone in between those two ITCZs. While the mean precipitation simulated in MOD is improved from STD in the northern Indian Ocean, the NATL, and the South Pacific Convergence Zone (SPCZ), the simulation is degraded in the Philippine Sea (Figure 1d, e). Overall, the modified convection scheme does not alter the systematic biases in the control simulation.

Although zonal-mean total precipitation also shows no significant change between the two simulations, they exhibit a different ratio of convective and stratiform precipitation (Figure 2). This suggests that the implementation of stochastic limit of entrainment rate tends to suppress deep convection and instead more rainfall is generated by large-scale condensation scheme. Held *et al.* (2007) and Lee *et al.* (2008) showed the sensitivity of large-scale stratiform precipitation to the minimum entrainment threshold increase

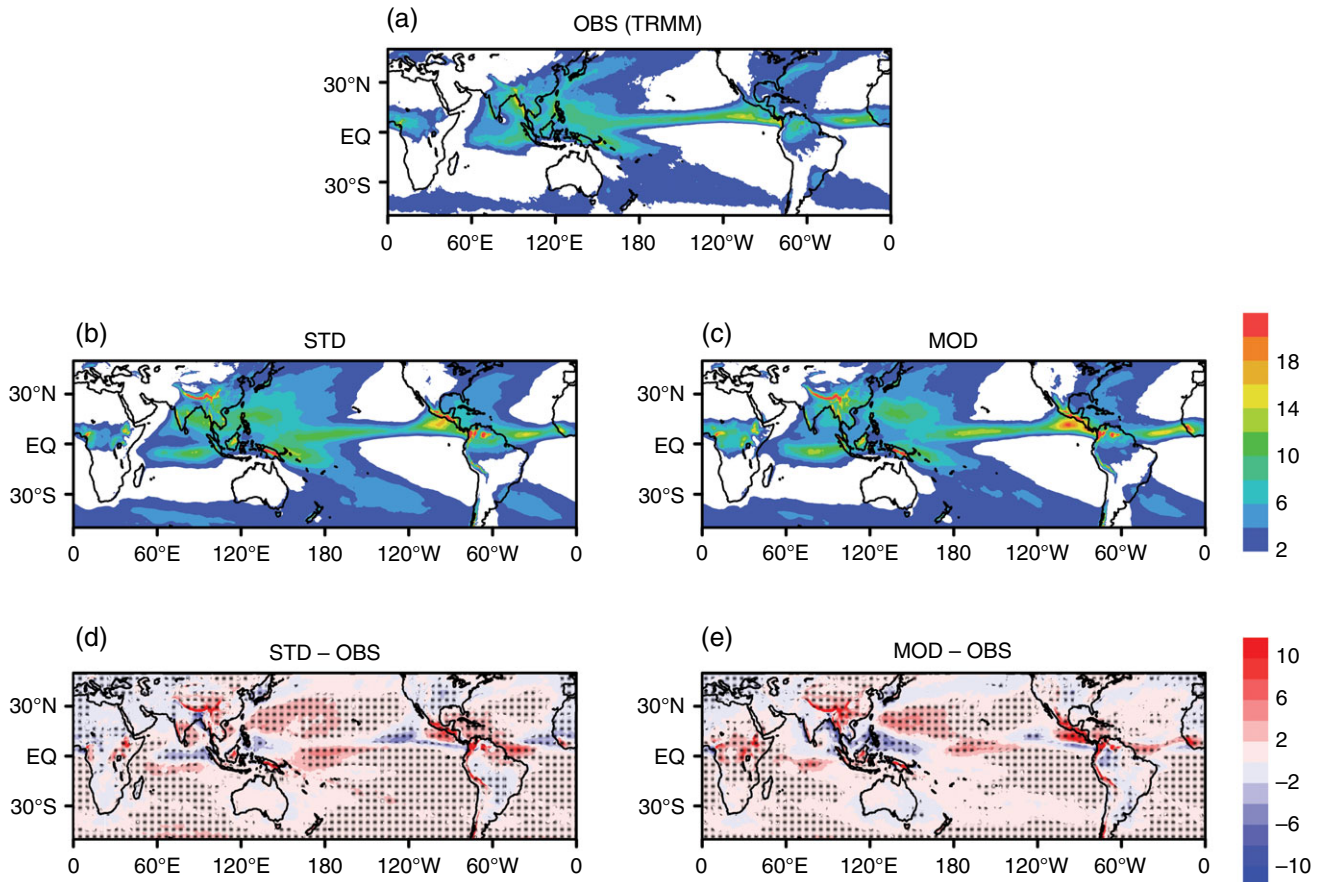


FIGURE 1 Precipitation (mm/day) climatology during June–October over 12 years (1998–2009) from (a) the observation, (b) “STD,” (c) “MOD,” (d) bias of “STD,” and (e) bias of “MOD.” Dotted area in (d, e) represents statistical significance at the 1% level from the Monte Carlo resampling test for 10,000 times

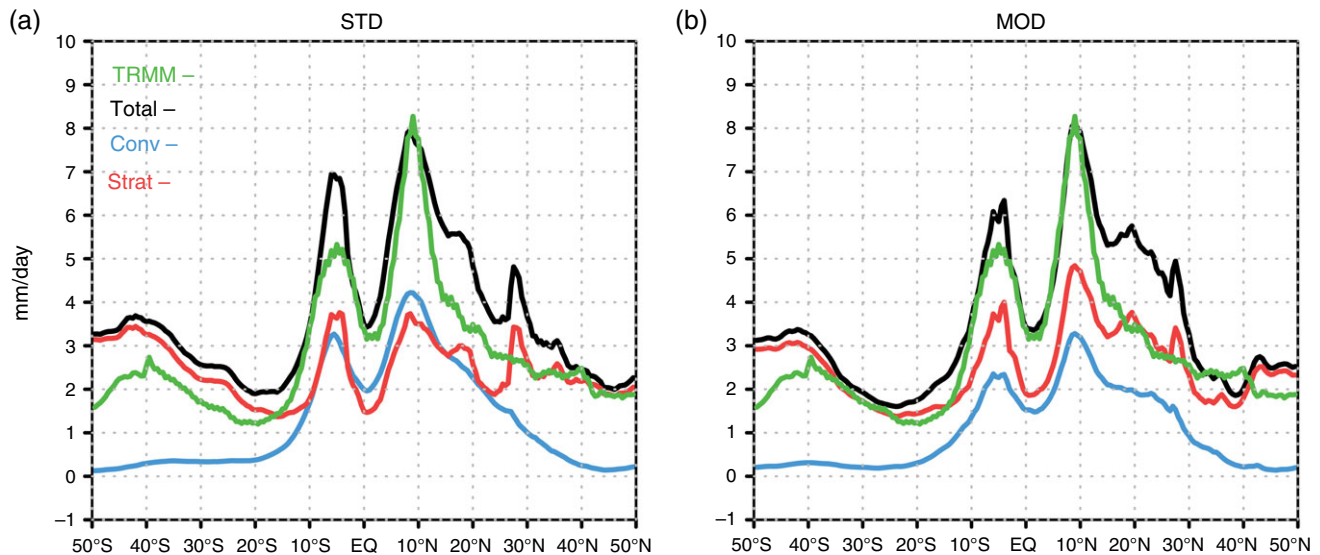


FIGURE 2 Zonal mean precipitation (mm/day) distribution for 12 years TC main development season (JJASO) simulated by GEOS-5 (a) “STD” and (b) “MOD” experiments. A green solid line represents the observation and the other line is the model result for each experiment (black, total precipitation; red, convective precipitation; blue, stratiform precipitation)

that suppresses deep convection. The simulated ratio of stratiform precipitation to total is changed from 50% in STD to 62% in MOD in the Tropics (20°S–20°N). This is comparable or somewhat larger than the observed value of about 40% estimated by Schumacher and Houze Jr (2003) using TRMM Precipitation Radar (PR) data, although the separation method is not exactly the same between the observation and the model simulation.

The modification in the convection scheme leads to significant changes in the vertical profile of temperature and humidity in the Tropics, thereby changing atmospheric vertical stability. Figure 3a is the zonal-mean vertical profiles of temperature over the Tropics (15°S–15°N), where both simulations show reliable vertical structure as compared with the MERRA reanalysis. STD reveals systematic warm biases in the boundary layer and the upper troposphere, whereas MOD shows overall cold bias through nearly the entire vertical column except near-surface level. MOD tends to reduce the overall moist bias in STD, leading to a more realistic humidity profile (Figure 3b). Increasing minimum entrainment threshold in the MOD simulation makes colder and drier than STD-produced atmosphere in the mid- to upper troposphere, likely due to less frequent convective adjustment and less vertical transport of energy and moisture by deep convection scheme. This process can decrease vertical stability in the simulated background state. As shown in Figure 3c, the modified convection scheme decreases the moist static energy (MSE) throughout the vertical column. Large reduction of MSE can effectively increase the convective available potential energy (CAPE) of rising plumes, which can provide a more favourable condition for strong convection once convection is occasionally triggered. The vertical gradient of equivalent potential temperature ($-d\theta_e/dp$) becomes more negative in lower levels and more

positive in upper levels, indicating an overall decrease of vertical stability in moist atmosphere (Figure 3d). This result is consistent with the result from Lim *et al.* (2015) where the modified convection scheme was tested at 25-km horizontal resolution. It is also noted that the modified convection scheme tends to simulate more realistic profiles of moisture, MSE, and $-d\theta_e/dp$.

Constraining convection scheme by increasing minimum entrainment threshold tends to increase the precipitation variability in an intra-seasonal timescale (e.g., Tokioka *et al.*, 1988; Lee *et al.*, 2003; Lee *et al.*, 2008; Lin *et al.*, 2008). This aspect is better illustrated in Figure 4, where we compare the simulated rainfall variance in the Tropics using timely-unfiltered daily precipitation data. The modified convection scheme tends to increase the rainfall variability significantly, while STD tends to underestimate the variance as compared with TRMM (cf., Figure 4a,c,e). In MOD, the rainfall variability has been increased particularly in the deep convection region including main development regions (MDRs) of TC in WNP and NATL. MDR refers to a region where TCs occur predominantly in WNP (0°–20°N, 115°–165°E) and NATL (10°–20°N, 20°–80°W). As will be discussed in the following sections, the simulated TC frequency has been increased substantially by the modified convection scheme, as well as with the significant increase in the TC intensity from the control simulation (not shown). It is interesting to note that the modification also increases low-frequency precipitation variability on subseasonal timescale of 20–100 days (cf., Figure 4b,d,f). This is a well-known feature by previous studies (e.g., Tokioka *et al.*, 1988; Lee *et al.*, 2003; Lin *et al.*, 2008; Jiang *et al.*, 2016), although the tested models are more or less different from one another.

In this timescale, the tropical atmosphere has a pronounced convective variability associated with the eastwards

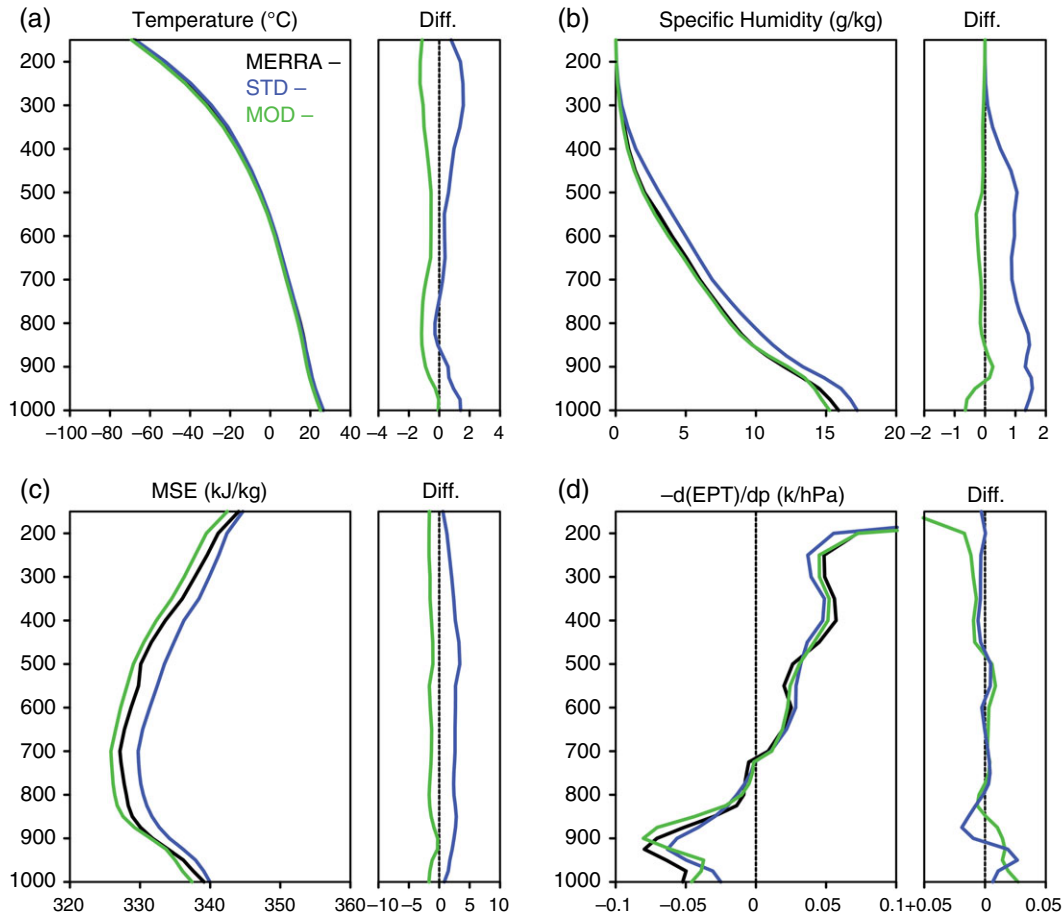


FIGURE 3 Vertical profile of (a) temperature (°C), (b) specific humidity ($10^{-3} \times \text{kg/kg}$), (c) MSE (kJ/kg), and (d) the vertical gradient of equivalent potential temperature (K/hPa) averaged over the Tropics ($0^\circ\text{--}360^\circ\text{E}$, $15^\circ\text{S}\text{--}15^\circ\text{N}$) and for the TC main development season (JJASO) for 12 years. MERRA reanalysis, “STD,” and “MOD” are represented by black, green, and blue line, respectively. Differences from MERRA for each model experiment are also provided on the right side of each figure

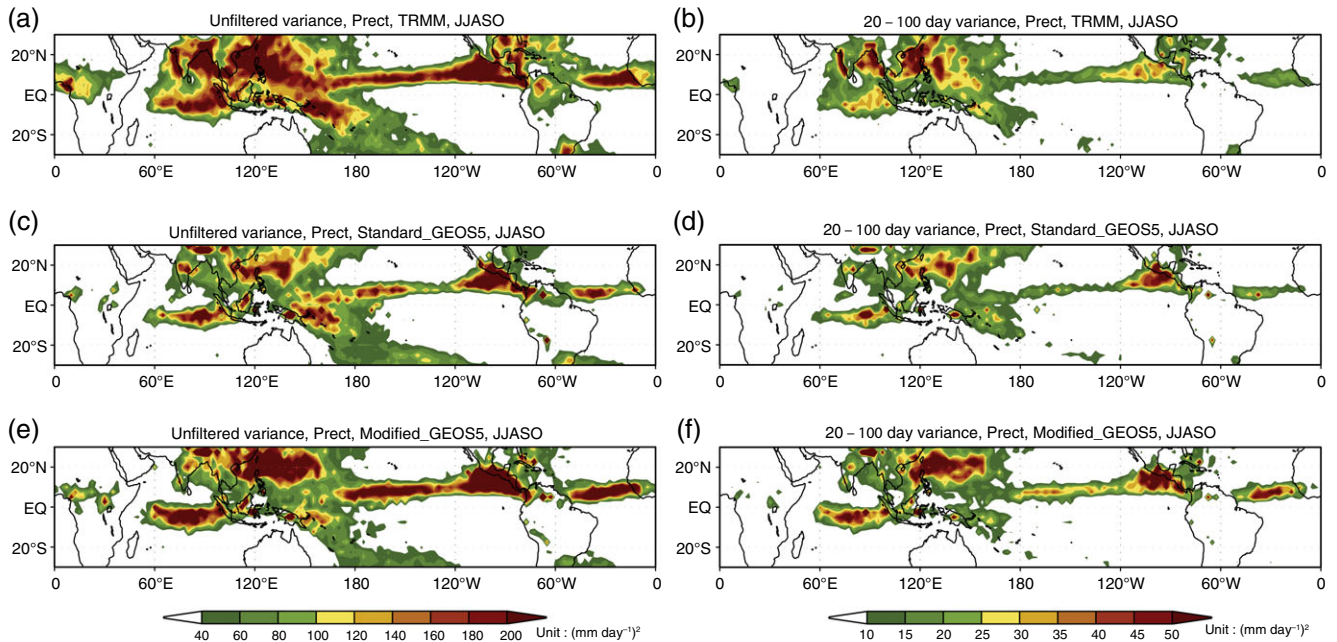


FIGURE 4 Unfiltered variance (left) and 20–100 days band-pass filtered (right) JJASO precipitation variance during 12 years for (a, b) TRMM observation, (c, d) “STD,” and (e, f) “MOD”

propagating Madden–Julian Oscillation (MJO), which also tends to influence development of TCs and their passages to

mid-latitudes. Figure 5 shows the eastwards propagation of MJO in the observation and the simulations, as examined

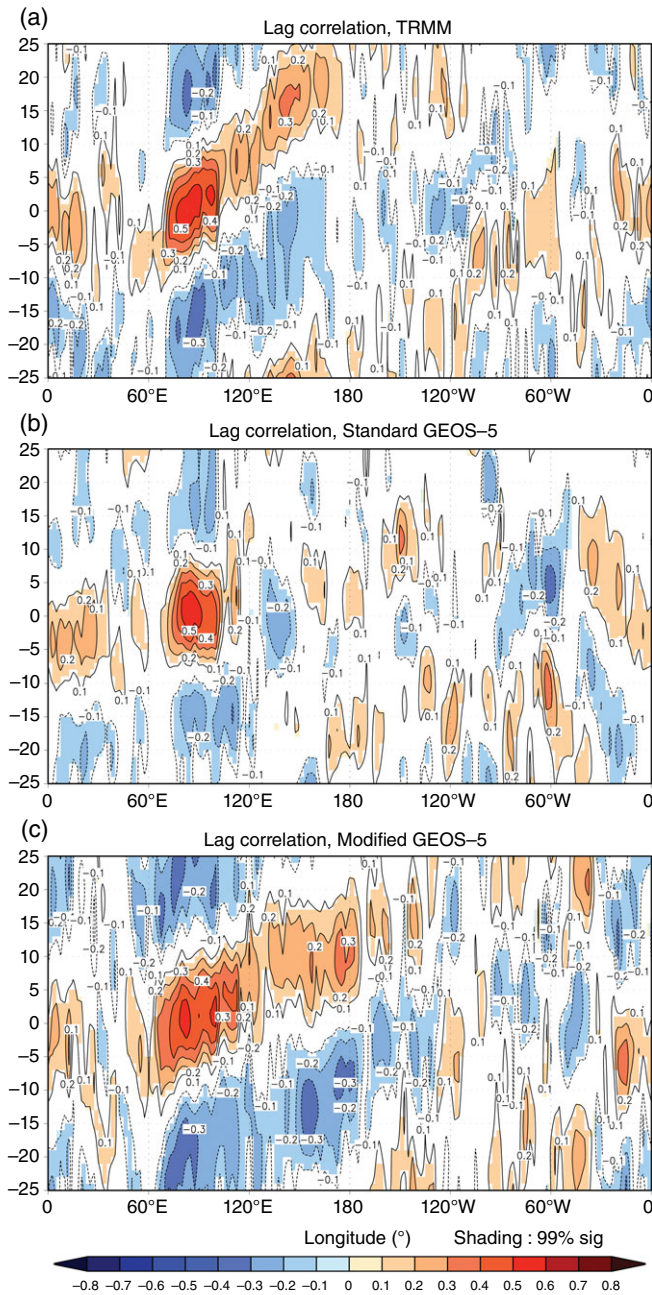


FIGURE 5 Lag correlation of 20–100 days band-pass filtered precipitation along the equator (10°N – 10°S) against base points at the Indian Ocean (70°E) for (a) the observation, (b) “STD,” and (c) “MOD”

with the lag correlations of the 20–100 days filtered daily precipitation along the equator (10°N – 10°S) with reference to the convection in the Indian Ocean (70°E) during JJASO. The TRMM observation clearly shows the eastwards propagation of active and suppressed convective signals which travel from the Indian Ocean to the central Pacific with a speed of about 5 m/s (Figure 5a). The propagation signal is marginal in STD. It is consistent with the previous MJO diagnostic study with climate models (Kim *et al.*, 2009), in which GEOS-5 control AMIP simulation did not reveal eastwards propagation. The feature is improved significantly in MOD with more realistic temporal evolution of tropical convection, particularly with the eastwards progression of MJO

across the Maritime Continent towards the Northwest Pacific. In another study using the same GEOS-5 model with the modified convection scheme (Kim *et al.*, 2014), the model was able to reproduce the modulation of TC activity by MJO realistically in the Northwest Pacific. Note that the simulated propagation speed is approximately 10 m/s, somewhat faster than the observed. This faster propagation speed is typical in most atmospheric GCMs driven by observed SST (Waliser *et al.*, 1999; Roundy and Kravitz, 2009), and it may be associated with a lack of air–sea interaction in the model.

3.2 | TC climatology

We next examine the realism of TCs simulated by the GEOS-5 model at 50-km horizontal resolution with the modified convection scheme, in terms of the genesis regions, tracks, and intensity of TCs, and the seasonal variation of the TC number over WNP and NATL, respectively. Simulation improvement by modified convection scheme is also examined by comparing the STD and the MOD runs.

Figure 6 shows the spatial distribution of TC genesis locations and tracks over WNP during May 15 to November 30 for the past 12 years (1998–2009). It is noted that MOD tends to improve the simulation of TC genesis number significantly. It produces 18.5 TCs per year on average, which is quite close to the observed value. However, the STD run produces only 11.2 TCs, which is about a half of the observed value. For the comparison of geographical distribution between the IBTrACs observation and two different model simulations (STD and MOD), TC numbers of genesis and track are counted in each $5^{\circ} \times 5^{\circ}$ grid box and then divided by the total number of TCs for the entire domain, respectively, to provide the normalized percentage frequencies. Observed TCs are mainly distributed over 110° – 170°E , 0° – 25°N (Figure 6a). The simulated genesis distribution by STD (Figure 6b) and MOD (Figure 6c) corresponds well to the observed distribution, although the MDR is shifted to the east. This bias is associated with the deficiency in the simulation of the time-mean climatology of mid-tropospheric vertical motion. The centre of upwards motion tends to be shifted to the east both in STD and MOD compared with the observation (see Figure S1, Supporting Information). The vertical motion in MOD becomes stronger in the MDR, which is a favourable condition for increasing TC genesis number. Simulated tracks seem to be realistic in both simulations, as they reproduce the main passage across the South China Sea and the east of the Philippines (Figure 6d,e,f). However, both simulations show the deficiency in the recurring TCs moving northeastwards after turning points. The geographical distribution of TC genesis and track simulated by MOD is broader than the case of STD, which seems to be related with the underestimation of TC number in the STD run with a single member.

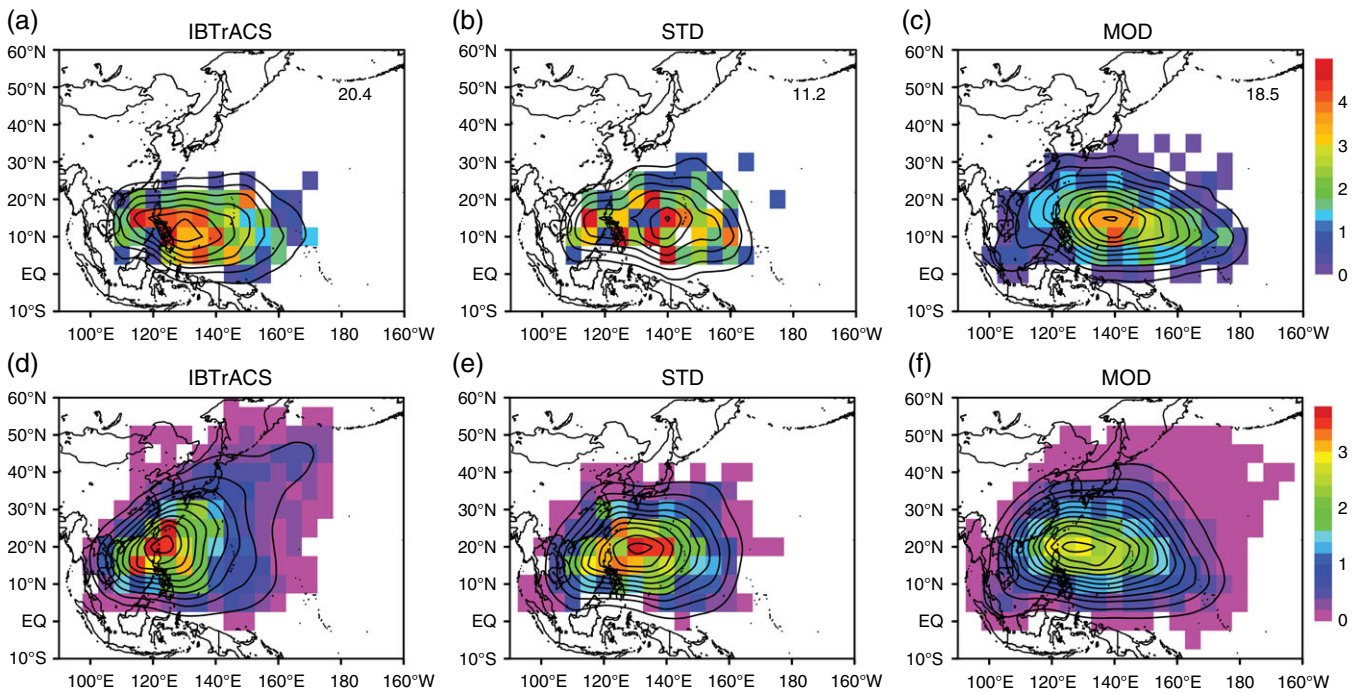


FIGURE 6 The percentage (%) of 12-year total (a–c) TC genesis (upper rows) and (d–f) track density (bottom rows) in WNP; IBTrACS (left), “STD” (middle), and “MOD” (right). The number in bold in each TC genesis map indicates the average annual TC number from observations and the model simulations

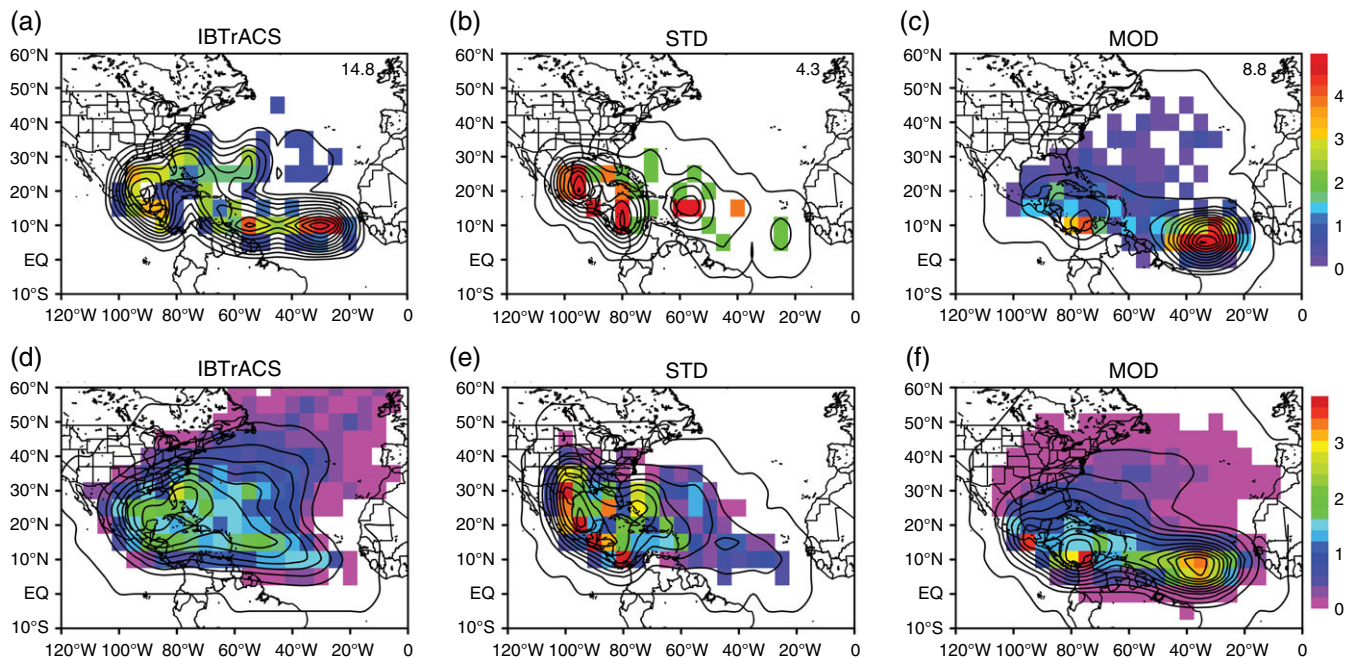


FIGURE 7 Same as Figure 6, but for NATL

In NATL, most of observed TCs are developed in the Gulf of Mexico, Caribbean Sea, and near the central Atlantic Ocean (Figure 7a). TC track density shows that the developed TCs are recurved along the western coast of Central America (Figure 7d). This observed feature is reasonably reproduced by both GEOS-5 experiments. Most of TCs simulated by STD are found over the Gulf of Mexico and the Caribbean Sea (Figure 7b), and they landfall over the southeastern United States and travel to the northern Mexico (Figure 7e). On the other hand, many of TCs reproduced by

MOD are found over the Caribbean Sea, and near the central Atlantic Ocean (Figure 7c), and landfalling TCs at the U.S. coast appear to weaken more rapidly than observations, showing relatively the lower track density values over the southeastern U.S. continent (Figure 7f). As in the case of WNP, the STD experiment also underestimates the TC genesis number in NATL. The TC genesis number has been increased by the modified convective parameterization (MOD). This result is consistent well with Lim *et al.* (2015), where the modified convection scheme leads to a substantial

increase in the TC frequency in this model run at 25-km horizontal resolution. It is noted that MOD still underestimates the TC genesis number over the basin, which seems to be related with the overall weak vertical motion simulated by the model over the entire NATL except for the tropical eastern area (see Figure S1). In particular, MOD tends to underestimate the TC genesis in the Gulf of Mexico, even smaller than STD, where the weak vertical motion bias becomes worse. On the other hand, TC genesis tends to be overpredicted in MOD over tropical NATL, which corresponds well to the unrealistically strong vertical motion in MOD over this region.

Figure 8 compares the PDF of the maximum 10-m wind speed and the minimum SLP, respectively, for individual TC lifetime by the IBTrACS best track data and two different GEOS-5 model experiments. The vertical dashed lines in maximum 10-m wind speed PDF represent regimes of the TC intensity scale (Saffir, 1977). MOD seems to simulate categories 2 and 3 in WNP whereas the observed PDF is widely spread till category 4, but STD cannot ever simulate category 1 (Figure 8a). The simulated minimum SLP is underestimated in WNP (Figure 8b). In NATL, MOD can resolve at most category 3 storms, where there are observed storms as intensive as category 5, even though STD is bounded at category 1 (Figure 8c). SLP is also systematically underestimated by the GEOS-5 model (Figure 8d). The TC intensity simulated by a GCM seems to depend on model physics parameterization as well as the horizontal resolution. Another 50-km resolution run by HiRAM (Zhao *et al.*, 2009) was able to simulate up to category 3 storms in WNP and NATL.

In addition, we explore the relationship between the 10-m maximum wind speed and minimum SLP in Figure 9. In the observation, the slope in WNP is steeper than NATL, which suggests that the decreasing rate of minimum SLP is larger in WNP at the increase of surface wind speed (Figure 9a,d). Stronger TCs are observed in NATL than in

WNP for the 12-year statistics. The observed maximum wind speed reaches up to 59 m/s in WNP and 82 m/s in NATL, with the minimum SLP of 900 and 882 hPa, respectively. In WNP, MOD shows realistic relationship between minimum SLP and maximum wind speed (Figure 9c). It can also reproduce realistic maximum wind speed, where minimum SLP reaches as low as 923 hPa and the maximum wind speed as high as 52 m/s, respectively. The MOD run also shows realistic relationship between minimum SLP and maximum wind speed, although the intensity is somewhat underestimated (Figure 9f). Obviously this is an improvement from STD in WNP (Figure 9b) and NATL (Figure 9e), which is made by the modified convection scheme. Lim *et al.* (2015) conducted a 25-km resolution run with the same model used in this study, which was able to resolve the TCs as intensified as 65 m/s in maximum wind speed in NATL. Putman and Suarez (2011) also addressed much finer horizontal resolution such as in 14-km is required to simulate TCs as strong as in the category 5.

Figure 10 compares the monthly variation of TC genesis number of the observation, STD, and MOD. In the observations, the TC genesis is at its maximum phase in August in WNP, while it peaks in September in NATL. MOD reproduces the observed peaks realistically both in August in WNP (Figure 10a) and in September in NATL (Figure 10b). The STD run is less realistic as it shows a less pronounced seasonal variation with an erroneous peak in October in WNP, and it also shows unrealistically sharp peak in September in NATL. Due to much smaller detected TCs in STD, it shows much weaker seasonal variation in TC genesis for both basins compared with the observations and MOD.

3.3 | Inter-annual variation

In this section, we compare the inter-annual variation of the variables that characterize the basin-wide TC activity. The

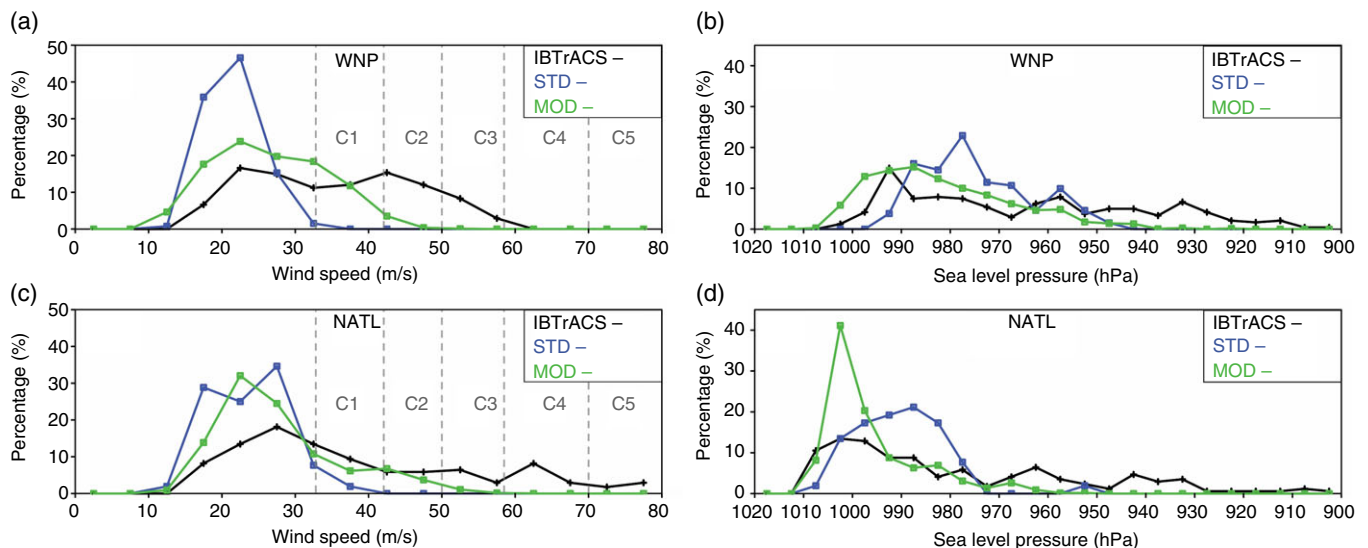


FIGURE 8 Comparison of the PDF (%) of the 10-m maximum surface wind speed and the minimum SLP of TCs between the observation (black), “STD” (blue), and “MOD” (green). (a, b) are for WNP and (c, d) for NATL

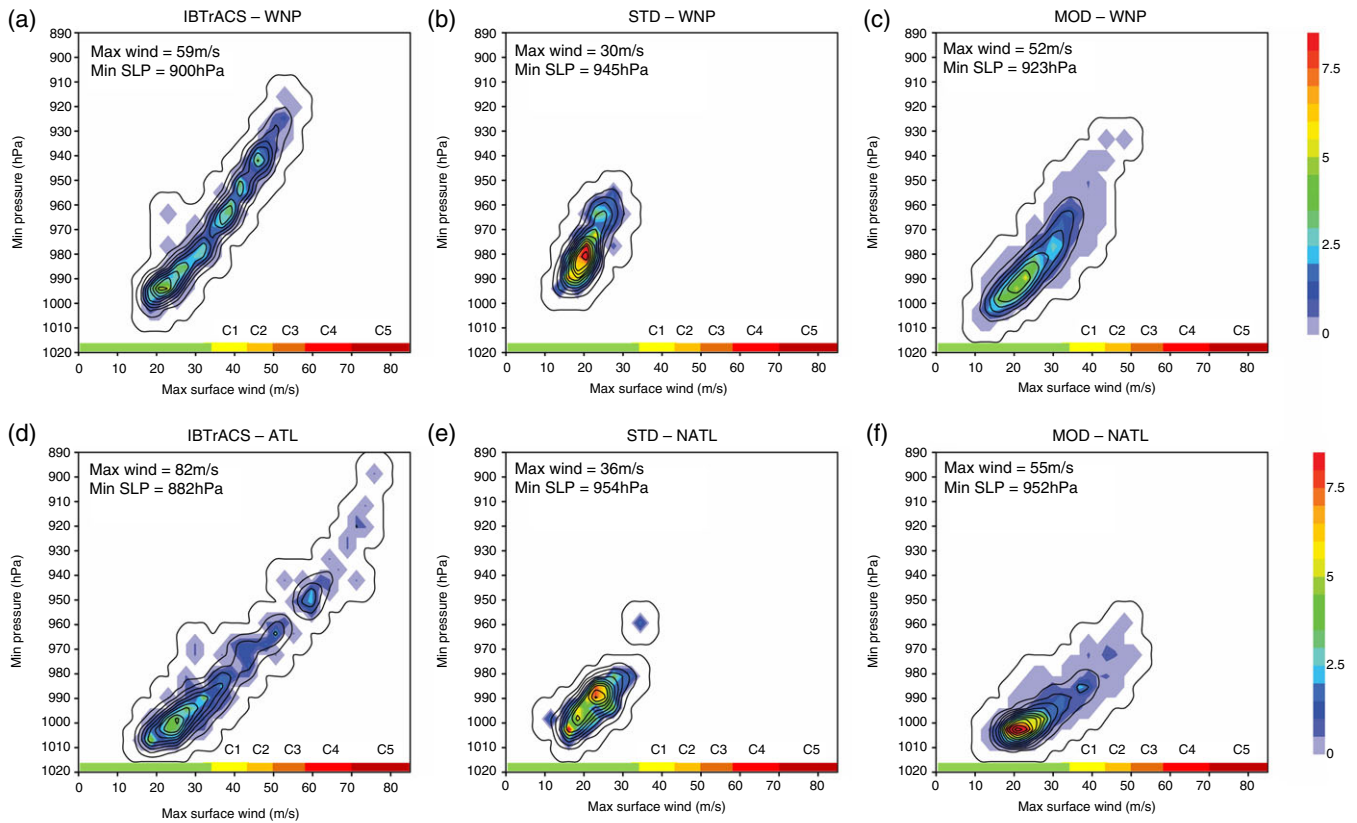


FIGURE 9 PDFs (%) of the relationship between 10-m maximum surface wind speed and minimum SLP for their maximum development phases. Upper panels are for WNP and low panels are for NATL (observations, “STD,” and “MOD” results are sequentially represented from the left column)

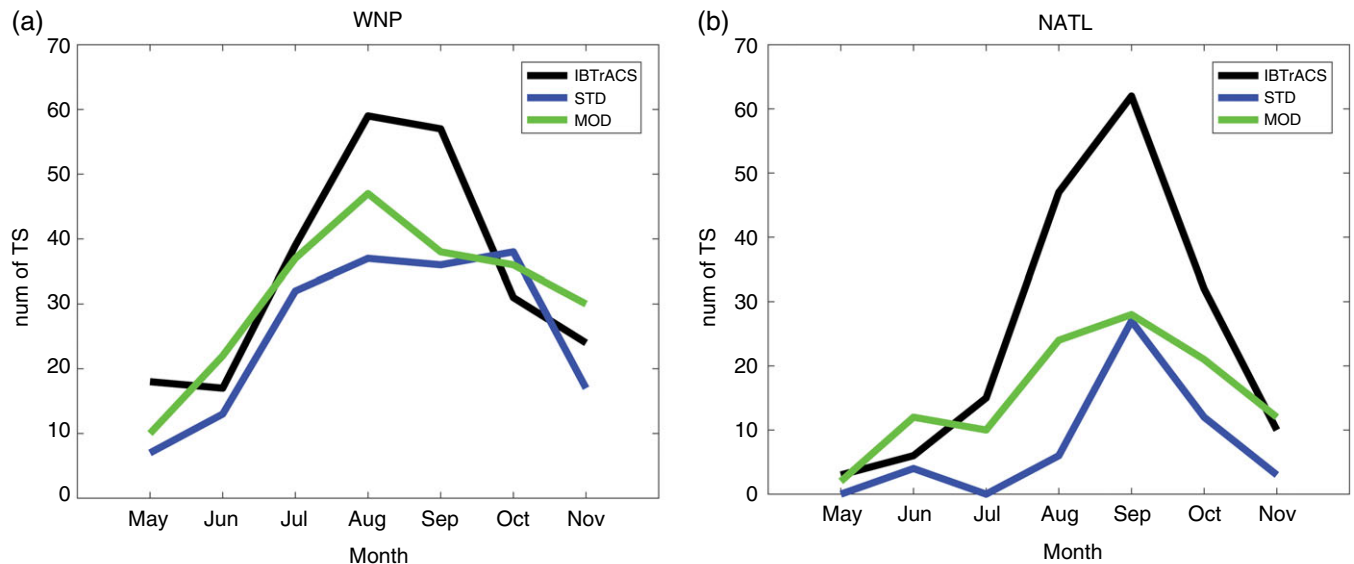


FIGURE 10 Seasonal cycle of the number of TC genesis from the observation (black), “STD” (blue), and “MOD” (green) for (a) WNP and (b) NATL. The values of the observation and single member “STD” run represent the averaged TC number each month for 12 years (1998–2009). “MOD” results represent the median values from the seasonal cycle of five ensemble runs that averaged for the same period

TC activity is represented by ACE, which can be decomposed into the individual TC intensity, and the duration for all TCs. The duration for all TCs can be further separated into the number TCs and the individual TC lifetime as derived in section 2.4.

Figures 11 and 12 show the year-to-year variation of ACE components for the observation and the model

simulations in WNP (Figure 11) and NATL (Figure 12), respectively. The figures show that STD has a significant underestimation for most of ACE components due to much smaller TCs simulated by STD. In MOD, the time series correlations have been improved and becomes statistically significant for most statistics in WNP (Table 1), although the correlation improvement is not notable in NATL. This

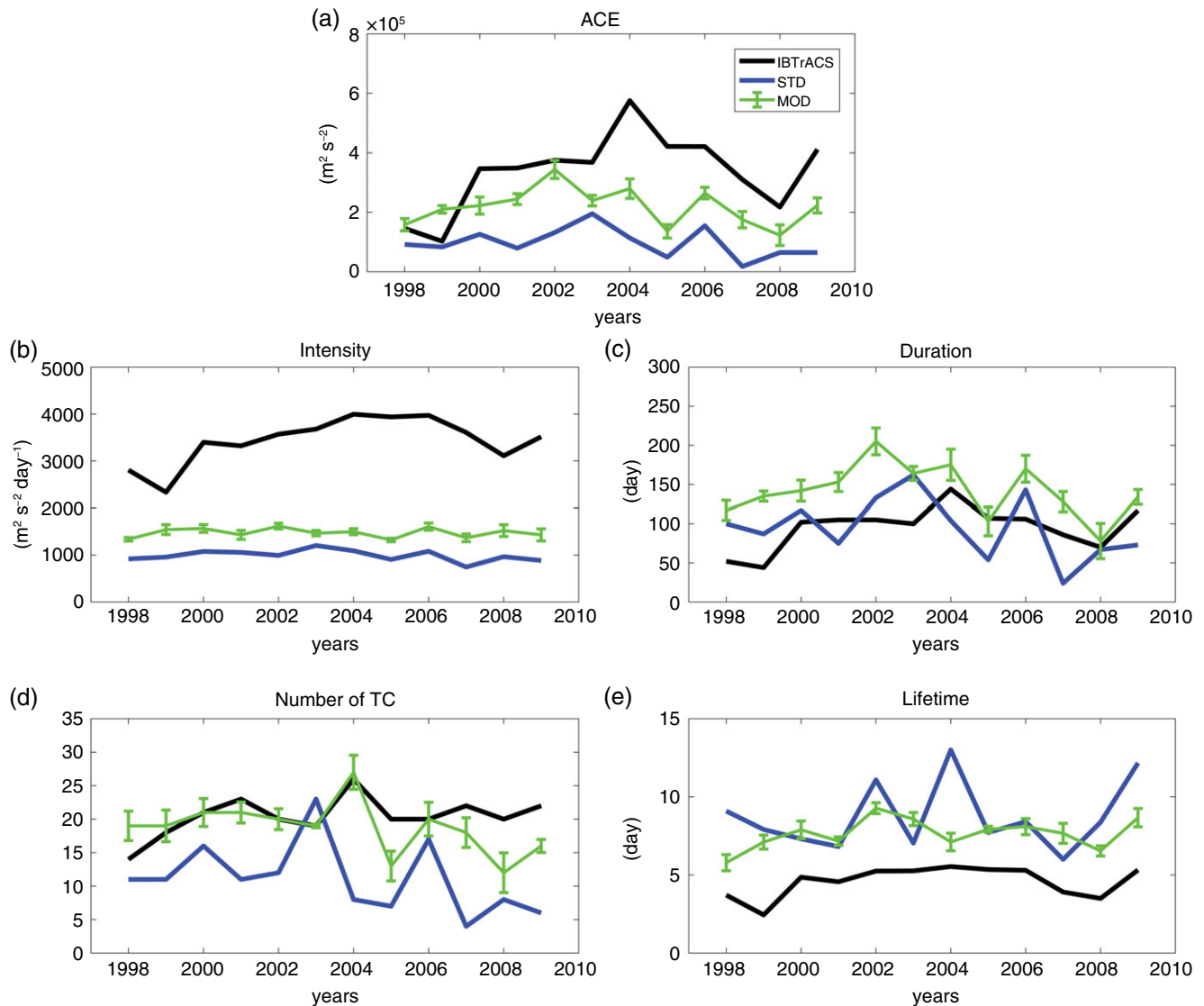


FIGURE 11 12 years (1998–2009) inter-annual variation of ACE components for the observation (black), “STD” (blue), and “MOD” (green) in WNP; (a) ACE, (b) intensity, (c) duration, (d) genesis numbers, and (e) individual lifetime. The model simulation is represented by the median values each year from the five ensemble runs. Each time series of the model is bounded by ± 1.0 standard deviation from the ensemble median value

basin-dependent sensitivity will be discussed later in the next subsection. The correlation coefficient (hereafter correlation coefficients of the detrended time series are given in parenthesis) for year-to-year variation of ACE in WNP is 0.46 (0.63) (Figure 11a). In this case, only the detrended correlation is statistically significant at the 95% confidence level. The correlation with the STD run is not statistically significant even with detrended time series ($r = 0.43$). On the other hand, the individual TC intensity is underestimated by the model with no significant correlation with the observed (Figure 11b), as the model has an intrinsic difficulty in reproducing the individual TC intensity as given in Figures 8 and 9. The inter-annual variability of ACE is mostly explained by that of TC duration (i.e., the total number of TC days). The correlation for the duration is 0.50 (0.67), where only the detrended correlation is statistically significant at the 95% confidence level (Figure 11c). When we separate the duration for all TCs into the number of TC

(Figure 11d) and the individual TC lifetime (Figure 11e), the correlation for the TC genesis number and the lifetime becomes 0.39 (0.74) and 0.62 (0.58), respectively. This suggests that the duration is more contributed by TC lifetime rather than TC number. The correlation with the TC genesis number is significant only for the case with the detrended time series. Correlation for the TC genesis number over WNP is comparable to the values obtained from other studies, which is around 0.5 by GFDL Atmospheric Model version 2.1 (AM2.1) (Zhao *et al.*, 2009), ECMWF Integrated Forecast System (IFS) (Manganello *et al.*, 2012), and MRI-AGCM version 3.1 and 3.2 (Murakami *et al.*, 2012). TC individual lifetime shows significant correlation regardless of trend in the time series, in spite of an overestimation of the lifetime for the entire analysis period. The problem is associated with the eastwards shift of TC genesis location in WNP (c.f. Figure 6c), which results in the extension of TC travelling time in the ocean.

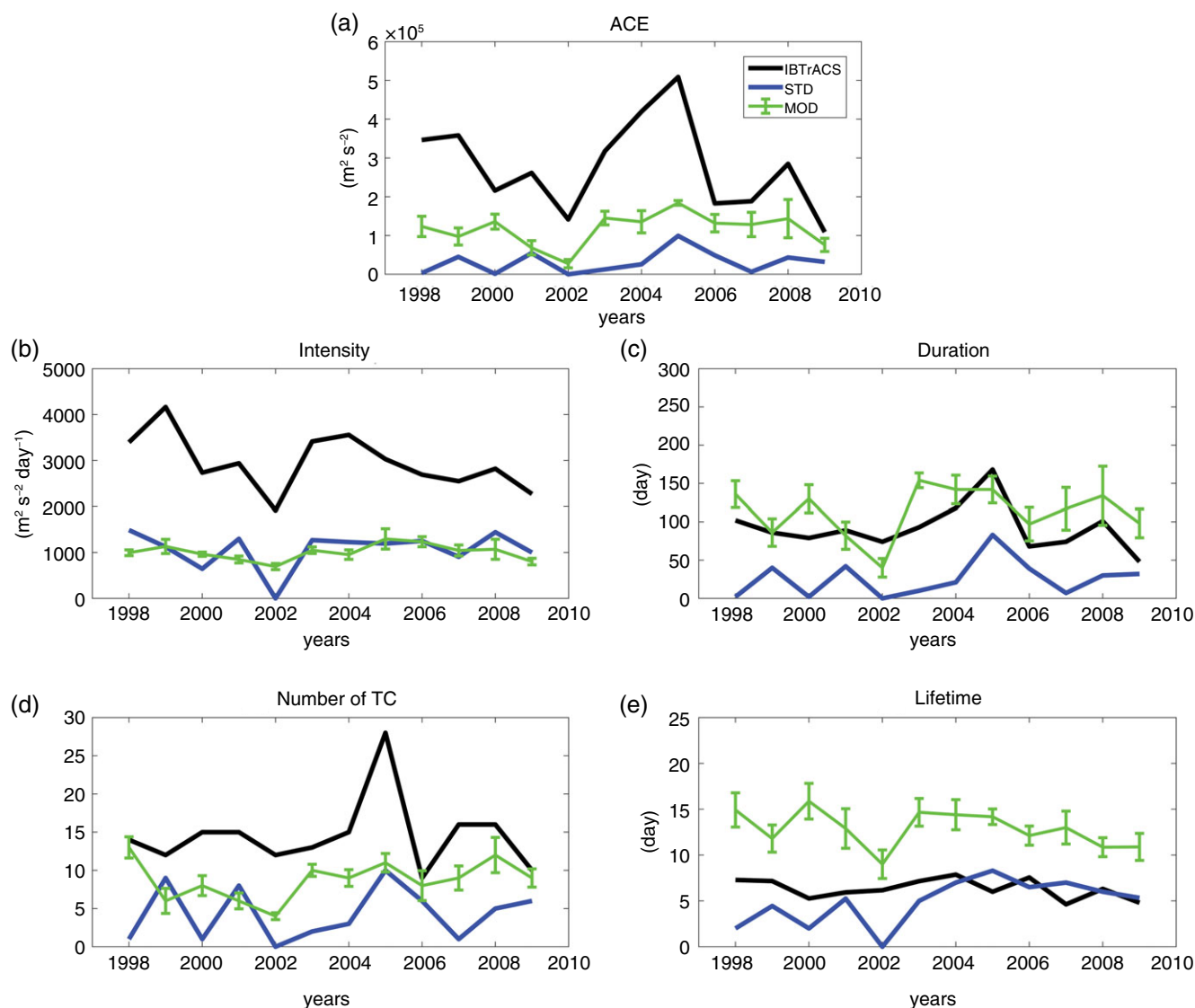


FIGURE 12 Same as Figure 11, but for NATL

TABLE 1 The correlation coefficient (detrended correlation is in parentheses) for 12 years (1998–2009) between the observation and GEOS-5 in WNP and NATL

	ACE	Individual intensity	Duration	No. of TC	Individual lifetime
WNP	0.46 (0.63*)	0.00 (0.04)	0.50 (0.67*)	0.39 (0.74**)	0.62* (0.58*)
NATL	0.63* (0.72**)	0.51 (0.61*)	0.47 (0.54)	0.38 (0.38)	0.16 (0.02)

Note. * is statistically significant at the 95% confidence level and ** indicates the confidence level over 99%.

Figure 12 compares the case of NATL. STD and MOD show statistically significant correlations for ACE with $r = 0.64$ and $r = 0.72$ for detrended time series, respectively. However, the discrepancy of ACE components between the observation and the model simulations becomes even larger than the case in WNP, in terms of magnitude and the year-to-year variation. While the discrepancy in magnitude between the observed and the simulated TC is mostly due to the underestimation of individual TC intensity in WNP, the simulated ACE magnitude over NATL is much smaller not only due to the underestimated individual intensity but also due to much less TCs in the model simulation. This is the

case for both STD and MOD runs, although the underestimation of TC number is particularly notable in STD.

Note that the individual TC lifetime is overall longer in the simulations over NATL. As shown in Figure 7c, the majority of TCs are generated in the central to eastern equatorial Atlantic in MOD, resulting in longer duration than the observed as they migrate towards the mid-latitudes. The correlation for ACE between the observed and the simulated is 0.63 (0.72), statistically significant at the 95 and 99% confidence level, respectively (Figure 12a). The correlation for the individual TC intensity is 0.51 (0.61), where only the detrended correlation is statistically significant at the 95%

confidence level (Figure 12b). On the other hand, the TC duration and its components show no significant correlation (Figure 12c). The model simulation does not reproduce a realistic inter-annual variability for the number TCs ($r = 0.38$ for the original and detrended time series) and the individual TC lifetime ($r = 0.16$ for the original and $r = 0.02$ for the detrended time series), where correlation values of them are statistically not significant (Figure 12d,e). Based on previous studies, correlation for the TC genesis number over NATL shows a large spread across the models, implying that the TC simulation is quite challenging in this region. Some models such as Florida State University (FSU) AGCM (LaRow *et al.*, 2008) and GFDL AM2.1 (Zhao *et al.*, 2009) show the correlation as good as 0.78 and 0.83, respectively, and other models such as EMCWF-IFS (Manganello *et al.*, 2012) and MRI-AGCM (Murakami *et al.*, 2012) exhibit the values around or below 0.5.

The correlation between the observed ACE and individual TC intensity, number of TC, and individual TC lifetime is, respectively, 0.86, 0.89, and 0.90 in WNP (if the correlation value is over 0.57, statistically significant at the 95% confidence level). The GEOS-5 tends to reproduce those observed relationship with the correlation values of 0.63, 0.75, and 0.57, respectively, all significant at the 95% confidence level. In NATL, the observed ACE is significantly related with individual TC intensity ($r = 0.71$) and number of TC ($r = 0.90$), but its relationship with the individual TC lifetime is not significant ($r = 0.32$). The model simulation

also shows significant correlations between simulated ACE and individual TC intensity ($r = 0.81$) and number of TC ($r = 0.83$) even though the correlation with the individual TC lifetime is high ($r = 0.76$). The GEOS-5 is able to reproduce the observed relationship between ACE and its components in both of basins. Therefore, the model driven by yearly varying SST boundary condition practically reproduces the inter-annual variation of the basin-wide ACE. However, the simulated correlations between ACE and its individual components are relatively weaker than the observed. This suggests there are still much room to improve the model simulation through improving the horizontal resolution and the physics parameterization.

3.4 | Sensitivity to ENSO

Bister and Emanuel (1998) pointed out the important role of oceanic SST forcing in increasing TC's kinetic energy. As the oceanic SST has a pronounced inter-annual variation due to ENSO, this study examines the TC sensitivity to ENSO, where the latter is represented by the SST anomalies over the Niño3.4 region (5°N – 5°S , 170° – 120°W) during the TC main development months (JJASO). When the Niño3.4 index becomes larger than 0.7, the year is classified as the El Niño year. The La Niña year is defined when the index is lower than -0.7 . During the 12 years (1998–2009) of investigation, there were four El Niño years (2002, 2004, 2006, and 2009) and four La Niña years (1998, 1999, 2000, and

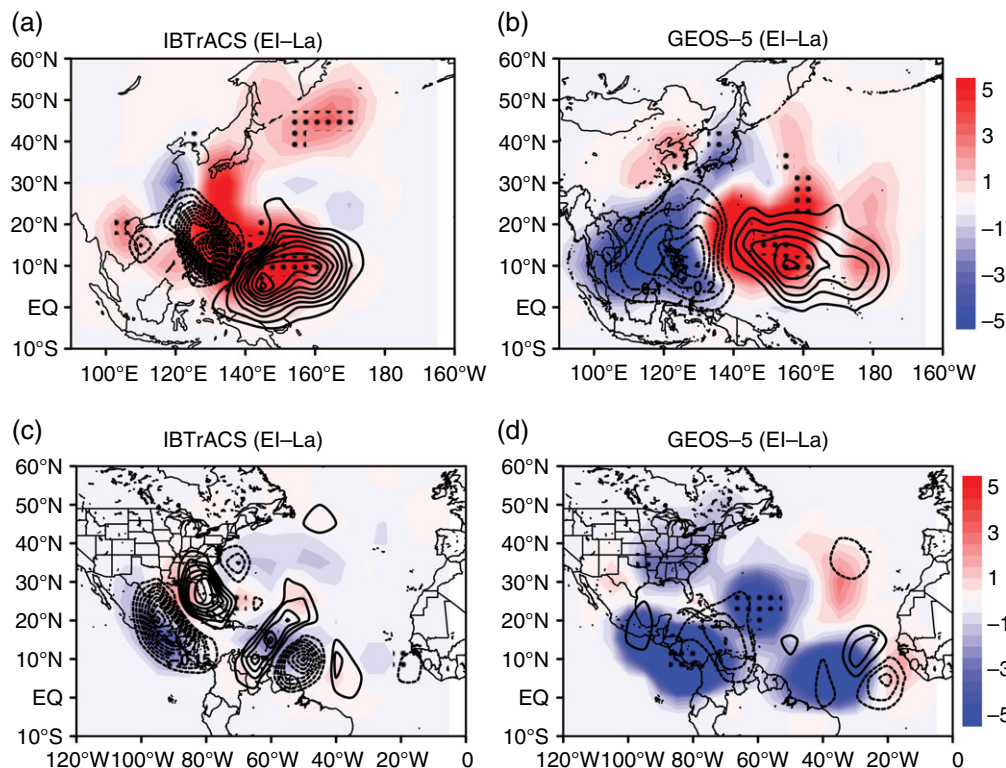


FIGURE 13 Difference maps of TC genesis (contour) and pathway (shading) between El Niño and La Niña in WNP (a) for the observation and (b) for the model simulation. (c, d) represents the case in NATL. Contour represents the genesis location anomaly; the contour interval is 0.05 (WNP) and 0.03 (NATL), and its style denotes the positive (solid) and negative (dashed) anomaly where the unit of shading and contour is number of TC per year

2007). The remaining years are classified as neutral years (2001, 2003, 2005, and 2008). The inter-annual variation of SST drives an anomalous Walker circulation, shifting areas of enhanced or suppressed convection and thereby changing the location of TC development and pathway (Kim *et al.*, 2011b; Zhang *et al.*, 2016).

Figure 13 shows the basin-wide difference map of TC pathway and origin between El Niño and La Niña, for the observation and the model simulation, respectively. Dotted area represents statistical significance of 10% level from the Monte Carlo resampling test for 10,000 times for TC pathway difference between El Niño and La Niña. During El Niño, the observed TCs are developed more in WNP (140° – 170° E), specifically to the east of the Philippines compared to La Niña. The pathway anomaly is also significantly positive in that region, along with the Philippine Sea and the East China Sea (Figure 13a). It also shows significantly negative anomalies in genesis over the Philippine Sea and in pathway over east coast of China. The GEOS-5 simulation tends to reproduce the observed pattern realistically, although the positive anomaly of TC genesis is shifted further east to the central Pacific (140° – 180° E) (Figure 13b). The model also shows strong negative anomalies of TC genesis over the Philippine Sea and the South China Sea and TC tracks travelling to those regions. The simulated patterns exhibit more robust sensitivity to the ENSO phase although the negative (positive) anomalous patterns tend to be shifted eastwards (westwards). It also shows negative anomalies in genesis and track in the South China Sea, which is overpredicted and not evident in the observations.

Sensitivity of TC activity to ENSO phase is quite opposite in NATL. During El Niño, the low-level convergence in the eastern Pacific leads to descending motion over the equatorial NATL, inhibiting TCs development in the region (Figure 13c). Large-scale subsidence driven by El Niño also results in the decrease of TC development over the Gulf of

Mexico and the Caribbean Sea (100° – 75° W). The model basically captures the observed sensitivity of TC activity to ENSO (Figure 13d). However, the negative genesis anomaly is underestimated in the model over the Gulf of Mexico and the Caribbean Sea. It is also noteworthy that the model exhibits too strong sensitivity in the negative pathway anomalies in most of NATL.

Figure 14 compares the correlation between Niño3.4 index and ACE components for the observation and the GEOS-5 simulation, respectively. In WNP, the observation shows that most of ACE components are significantly associated with the Niño3.4 SST (Figure 14a). The model also reveals the strong relation between Niño3.4 SST and the ACE. This strong ENSO relationship can be attributed to the duration rather than the individual TC intensity, and the duration is mainly explained by the individual TC lifetime rather than the number of TCs. The weak relationship with the individual TC intensity may be associated with the model deficiency that has a limitation to realistically resolve intense TCs. On the contrary, correlations for NATL region are overall negative, indicating that ACE components are smaller (larger) during El Niño (La Niña), though the correlation values do not appear statistically significant in both the observation and the model (Figure 14b).

The weak relationship between ENSO and the TC activity in NATL seems to be in part related to our relatively short analysis period. Note that the observed sensitivity to ENSO in the TC pathway anomaly in NATL is not as strong as in WNP, showing much less area of statistical significance (cf., Figure 13a,c). The TC genesis anomaly also shows a less coherent spatial pattern. In our investigation, the negative ENSO relationship with TC activities in NATL becomes weak in recent years (1998–2009) due to the positive phase of the Atlantic Multidecadal Oscillation (AMO; see Figure S2). The positive AMO is known to provide more favourable conditions for enhanced NATL TC activity such

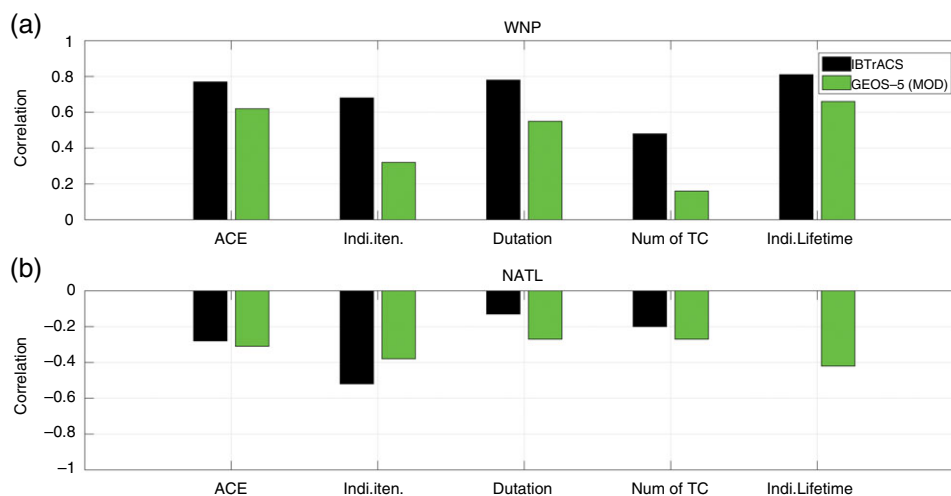


FIGURE 14 (a) The correlation coefficient between the observed Niño3.4 SST and ACE components by the observation (black) and the GEOS-5 model (green) for 12 years (1998–2009) in WNP. (b) Is for NATL. Five-member ensemble medians were taken for the model results. (± 0.57 value is statistically significant at the 95% confidence level)

as through decreased vertical wind shear and increased CAPE (Vimont and Kossin, 2007; Wang *et al.*, 2008; Klotzbach, 2011). Based on the long-term analysis period (1982–2009), the ENSO variability shows a statistically significant relationship with much suppressed ACE and reduced TC number in NATL (Figure S2b), suggesting a decadal modulation of TC activity by AMO (Roberts *et al.*, 2015). The GEOS-5 model exhibits a fundamental limitation in reproducing this observed decadal change (Figure S3).

4 | SUMMARY AND CONCLUSION

This study has examined the role of deep convective activity modified in the RAS-based convective scheme in modulating TC activity over the WNP and NATL. GEOS-5 AGCM run is carried out at 50-km spatial resolution over 12 years (1998–2009). We vary the minimum entrainment threshold through the stochastic limit to suppress the parameterized deep convection. The minimum entrainment rate (λ_0) is defined by $\lambda_0 = \alpha/D_m$ and dependent of the term D_m that represents the sub-cloud layer, which is related to the plume radius. Small D_m indicates high λ_0 , equivalent with enhanced entrainment threshold that more severely limits the parameterized convection. It leads to more active grid-scale condensation and stratiform precipitation. The experiment applying the stochastic minimum entrainment threshold, “MOD,” shows the increasing convective variability and improving TC simulations without the large change in seasonal mean climates over TC MDR. Total precipitation climatology is not substantially changed even though the process of organizing deep convection is considerably modified. Convective precipitation is suppressed in the Tropics, but resolved-scale stratiform precipitation increases to compensate for reduction in sub-grid-scale convective precipitation. The modified convection scheme acts to decrease the MSE throughout the vertical column and atmospheric vertical stability. Large reduction of MSE increases CAPE of rising plumes, providing more favourable conditions for strong convection once convection is occasionally triggered. Constraining convection scheme by increasing minimum entrainment threshold tends to increase the precipitation variability.

The five-member ensemble simulations using the GEOS-5 model with the T convective scheme also achieve significant improvements in the TC simulation. This improvement is mostly attributed to the more realistic simulation of the model basic state such as vertical motion in the mid-troposphere. The modified version of GEOS-5 tends to increase the overall convective variability and the TC number and intensity as well (e.g., maximum surface wind speed and minimum SLP). It can simulate tropical storms categorized up to 3 in both basins, whereas the original version of the model barely simulates the storms in category 1. The ensemble MOD runs reliably capture the TC MDR in WNP (e.g., the South China Sea and the east of the Philippines)

and NATL (e.g., the Caribbean Sea, and near the central Atlantic Ocean). The inter-annual variation of basin-wide TC activities is investigated focusing on ACE, duration, intensity, TC numbers, and individual TC lifetime. The result demonstrates that inter-annual variation of the ACE and the duration are reasonably simulated by GEOS-5, which implies that the GCM prescribing year-to-year varying observed SST can significantly resolve the TC features. However, the GEOS-5 model exhibits notable, basin-dependent discrepancy as well in reproducing the observed inter-annual variation of TC activity and the sensitivity to ENSO. It performs relatively better in WNP with a skill comparable to other GCMs. The model also reproduces the observed sensitivity of spatial feature of TCs and the basin-wide observed ACE variability associated with ENSO realistically. On the other hand, it performs poorly in NATL, which seems to be a weakness of this model. Comparing with the results from previous studies, TC simulations over NATL shows a large spread across the models, implying that the TC simulation is quite challenging in this region. This deficiency is insensitive to the simulation period, in which the model is not able to reproduce the observed decadal modulation of the relationship between ENSO and NATL TC activity through AMO.

The model simulation in this study with 50-km grid spatial resolution shows a fundamental limitation in resolving realistically the intensive TCs. This problem is common in the TC simulation by GCMs (Shaevitz *et al.*, 2014). Some of previous studies addressed the problem could be solved by enhancing the spatial resolution or model physics of AGCM (Manganello *et al.*, 2012; Murakami *et al.*, 2012; Murakami *et al.*, 2015; Roberts *et al.*, 2015). Putman and Suarez (2011) performed TC simulations with much higher resolution (14 and 7 km) GEOS-5 model, which realistically simulates the intense TC. However, there is a difficulty in performing ultra-high resolution ensemble experiments due to the limited computing resources. Improving convective parameterization is an alternative approach to simulate realistic TC activity with limited horizontal resolution. Lim *et al.* (2015) showed that modification of convective parameterization improves simulation of intense TCs (up to categories 3 and 4), with little changing the seasonal mean climate, while another model simulation without changing convection scheme resolved only up to category 2 TC. As such, this study addresses the importance of convective parameterization to better resolve the TCs in numerical model and their inter-annual variations through multi-year ensemble member runs. Our results suggest much of the inter-model differences appeared in the previous high-resolution GCM intercomparison studies could be attributed to the convection schemes implemented differently across the GCMs. Of course, this seems to be the case for the models run at similar horizontal resolution, but the

convection scheme is one of the highest priorities to improve in addition to the resolution increase.

This study also highlights that the improvement of the TC simulation can be attained under more realistic representation in the time-mean state and MJO variability. The so-called, “MJO paradox” has been a widely recognized problem in the GCM modelling community (Kim *et al.*, 2011b; Yoo *et al.*, 2015), in which there is a trade-off in improvement between time-mean state and temporal variability such as MJO. The stochastic limit of the minimum entrainment rate of convective plumes tends to improve the overall convective variability not only the intensity of the TC-like disturbances but also the MJO amplitude, even with no significant degradation in the basic state. In this regard, the impact of the stochastic parameterizations is worth more in-depth researches.

ACKNOWLEDGEMENTS

This study was supported by the Korea Meteorological Administration Research and Development Program under Grant KMI2018-03110.

ORCID

Eunkyo Seo  <https://orcid.org/0000-0002-3517-3054>

REFERENCES

- Bacmeister, J. and Stephens, G. (2011) Spatial statistics of likely convective clouds in CloudSat data. *Journal of Geophysical Research: Atmospheres*, 116(D4), D04104.
- Bengtsson, L., Böttger, H. and Kanamitsu, M. (1982) Simulation of hurricane-type vortices in a general circulation model. *Tellus A*, 34(5), 440–457.
- Bengtsson, L., Hodges, K. and Esch, M. (2007) Tropical cyclones in a T159 resolution global climate model: comparison with observations and re-analyses. *Tellus A*, 59(4), 396–416.
- Bister, M. and Emanuel, K.A. (1998) Dissipative heating and hurricane intensity. *Meteorology and Atmospheric Physics*, 65(3), 233–240.
- Camargo, S.J. and Sobel, A.H. (2005) Western North Pacific tropical cyclone intensity and ENSO. *Journal of Climate*, 18(15), 2996–3006.
- Camargo, S.J. and Zebiak, S.E. (2002) Improving the detection and tracking of tropical cyclones in atmospheric general circulation models. *Weather and forecasting*, 17(6), 1152–1162.
- Chan, J.C. (1985) Tropical cyclone activity in the Northwest Pacific in relation to the El Niño/Southern Oscillation phenomenon. *Monthly Weather Review*, 113(4), 599–606.
- Chen, J.H. and Lin, S.J. (2011) The remarkable predictability of inter-annual variability of Atlantic hurricanes during the past decade. *Geophysical Research Letters*, 38(11), L11804.
- Emanuel, K. (2005) Increasing destructiveness of tropical cyclones over the past 30 years. *Nature*, 436(7051), 686–688.
- Han, R., Wang, H., Hu, Z.-Z., Kumar, A., Li, W., Long, L.N., Schemm, J.-K.E., Peng, P., Wang, W. and Si, D. (2016) An assessment of multimodel simulations for the variability of western North Pacific tropical cyclones and its association with ENSO. *Journal of Climate*, 29(18), 6401–6423.
- Held, I.M., Zhao, M. and Wyman, B. (2007) Dynamic radiative–convective equilibria using GCM column physics. *Journal of the atmospheric sciences*, 64(1), 228–238.
- Huffman, G.J., Bolvin, D.T., Nelkin, E.J., Wolff, D.B., Adler, R.F., Gu, G., Hong, Y., Bowman, K.P. and Stocker, E.F. (2007) The TRMM multisatellite precipitation analysis (TMPA): quasi-global, multiyear, combined-sensor precipitation estimates at fine scales. *Journal of Hydrometeorology*, 8(1), 38–55.
- Jiang, X., Zhao, M., Maloney, E. D., Waliser, D. E. (2016) Convective moisture adjustment time scale as a key factor in regulating model amplitude of the Madden-Julian Oscillation. *Geophysical Research Letters*, 43.
- Kang, S.M., Held, I.M., Frierson, D.M. and Zhao, M. (2008) The response of the ITCZ to extratropical thermal forcing: idealized slab-ocean experiments with a GCM. *Journal of Climate*, 21(14), 3521–3532.
- Kim, D., Lee, M.I., Kim, H.M., Schubert, S.D. and Yoo, J.H. (2014) The modulation of tropical storm activity in the western North Pacific by the Madden-Julian Oscillation in GEOS-5 AGCM experiments. *Atmospheric Science Letters*, 15(4), 335–341.
- Kim, D., Sobel, A.H., Maloney, E.D., Frierson, D.M. and Kang, I.-S. (2011b) A systematic relationship between intraseasonal variability and mean state bias in AGCM simulations. *Journal of Climate*, 24(21), 5506–5520.
- Kim, D., Sperber, K., Stern, W., Waliser, D., Kang, I.-S., Maloney, E., Wang, W., Weickmann, K., Benedict, J. and Khairoutdinov, M. (2009) Application of MJO simulation diagnostics to climate models. *Journal of Climate*, 22(23), 6413–6436.
- Kim, H.-M., Webster, P.J. and Curry, J.A. (2011a) Modulation of North Pacific tropical cyclone activity by three phases of ENSO. *Journal of Climate*, 24(6), 1839–1849.
- Klotzbach, P.J. (2011) The influence of El Niño–Southern Oscillation and the Atlantic Multidecadal Oscillation on Caribbean tropical cyclone activity. *Journal of Climate*, 24(3), 721–731.
- Knap, K.R., Kruk, M.C., Levinson, D.H., Diamond, H.J. and Neumann, C.J. (2010) The international best track archive for climate stewardship (IBTrACS) unifying tropical cyclone data. *Bulletin of the American Meteorological Society*, 91(3), 363–376.
- LaRow, T., Lim, Y., Shin, D., Chassignet, E. and Cocke, S. (2008) Atlantic basin seasonal hurricane simulations. *Journal of Climate*, 21(13), 3191–3206.
- Lee, M.-I., Kang, I.-S. and Mapes, B.E. (2003) Impacts of cumulus convection parameterization on aqua-planet AGCM simulations of tropical intraseasonal variability. *Journal of the Meteorological Society of Japan*, 81, 963–992.
- Lee, M.-I., Suarez, M.J., Kang, I.-S., Held, I.M. and Kim, D. (2008) A moist benchmark calculation for atmospheric general circulation models. *Journal of Climate*, 21(19), 4934–4954.
- Lim, Y.-K., Schubert, S.D., Reale, O., Lee, M.-I., Molod, A.M. and Suarez, M.J. (2015) Sensitivity of tropical cyclones to parameterized convection in the NASA GEOS-5 model. *Journal of Climate*, 28(2), 551–573.
- Lin, J.-L., Lee, M.-I., Kim, D., Kang, I.-S. and Frierson, D.M. (2008) The impacts of convective parameterization and moisture triggering on AGCM-simulated convectively coupled equatorial waves. *Journal of Climate*, 21(5), 883–909.
- Manabe, S., Holloway, J.L., Jr. and Stone, H.M. (1970) Tropical circulation in a time-integration of a global model of the atmosphere. *Journal of the Atmospheric Sciences*, 27(4), 580–613.
- Manganello, J.V., Hodges, K.I., Kinter, J.L., III, Cash, B.A., Marx, L., Jung, T., Achuthavarier, D., Adams, J.M., Altschuler, E.L. and Huang, B. (2012) Tropical cyclone climatology in a 10-km global atmospheric GCM: toward weather-resolving climate modeling. *Journal of Climate*, 25(11), 3867–3893.
- Matsuura, T., Yumoto, M., Iizuka, S. and Kawamura, R. (1999) Typhoon and ENSO simulation using a high-resolution coupled GCM. *Geophysical Research Letters*, 26(12), 1755–1758.
- Mei, W., Xie, S. P. and Zhao, M. (2014) Variability of tropical cyclone track density in the North Atlantic: Observations and high-resolution simulations. *Journal of Climate*, 27(13), 4797–4814.
- Mei, W., Xie, S. P., Zhao, M., and Wang, Y. (2015) *Forced and internal variability of tropical cyclone track density in the western North Pacific*. *Journal of Climate*, 28(1), 143–167.
- Molod, A., Takacs, L., Suarez, M., Bacmeister, J., Song, I.-S., and Eichmann, A. (2012) *The GEOS-5 Atmospheric General Circulation Model: Mean Climate and Development from MERRA to Fortuna*. NASA Tech. Rep. TM-2012-104606, 28, 117.
- Moorthi, S. and Suarez, M.J. (1992) Relaxed Arakawa-Schubert. A parameterization of moist convection for general circulation models. *Monthly Weather Review*, 120(6), 978–1002.
- Murakami, H., Vecchi, G.A., Underwood, S., Delworth, T.L., Wittenberg, A.T., Anderson, W.G., Chen, J.-H., Gudgel, R.G., Harris, L.M. and Lin, S.-J. (2015) Simulation and prediction of category 4 and 5 hurricanes in the high-resolution GFDL HiFLOR coupled climate model. *Journal of Climate*, 28(23), 9058–9079.

- Murakami, H., Wang, Y., Yoshimura, H., Mizuta, R., Sugi, M., Shindo, E., Adachi, Y., Yukimoto, S., Hosaka, M. and Kusunoki, S. (2012) Future changes in tropical cyclone activity projected by the new high-resolution MRI-AGCM. *Journal of Climate*, 25(9), 3237–3260.
- Putman, W.M. and Suarez, M. (2011) Cloud-system resolving simulations with the NASA Goddard Earth Observing System global atmospheric model (GEOS-5). *Geophysical Research Letters*, 38(16), L16809.
- Rayner, N., Parker, D.E., Horton, E., Folland, C., Alexander, L., Rowell, D., Kent, E. and Kaplan, A. (2003) Global analyses of sea surface temperature, sea ice, and night marine air temperature since the late nineteenth century. *Journal of Geophysical Research: Atmospheres*, 108(D14), 4407.
- Reynolds, R.W., Rayner, N.A., Smith, T.M., Stokes, D.C. and Wang, W. (2002) An improved in situ and satellite SST analysis for climate. *Journal of Climate*, 15(13), 1609–1625.
- Rienecker, M.M., Suarez, M.J., Gelaro, R., Todling, R., Bacmeister, J., Liu, E., Bosilovich, M.G., Schubert, S.D., Takacs, L. and Kim, G.-K. (2011) MERRA: NASA's Modern-Era Retrospective analysis for research and applications. *Journal of Climate*, 24(14), 3624–3648.
- Roberts, M.J., Vidale, P.L., Mizielinski, M.S., Demory, M.-E., Schiemann, R., Strachan, J., Hodges, K., Bell, R. and Camp, J. (2015) Tropical cyclones in the UPSCALE ensemble of high-resolution global climate models. *Journal of Climate*, 28(2), 574–596.
- Roundy, P.E. and Kravitz, J.R. (2009) The association of the evolution of intra-seasonal oscillations to ENSO phase. *Journal of Climate*, 22(2), 381–395.
- Saffir, H. S. (1977) *Design and construction requirements for hurricane resistant construction*. American Society Civil Engineers Tech. Rep. Preprint 2830, 20.
- Sanderson, B.M., Piani, C., Ingram, W., Stone, D. and Allen, M. (2008) Towards constraining climate sensitivity by linear analysis of feedback patterns in thousands of perturbed-physics GCM simulations. *Climate Dynamics*, 30 (2–3), 175–190.
- Schumacher, C. and Houze, R.A., Jr. (2003) Stratiform rain in the Tropics as seen by the TRMM precipitation radar. *Journal of Climate*, 16(11), 1739–1756.
- Shaevitz, D.A., Camargo, S.J., Sobel, A.H., Jonas, J.A., Kim, D., Kumar, A., LaRow, T.E., Lim, Y.-K., Murakami, H. and Reed, K.A. (2014) Characteristics of tropical cyclones in high-resolution models in the present climate. *Journal of Advances in Modeling Earth Systems*, 6(4), 1154–1172.
- Simpson, J. and Wiggert, V. (1969) Models of precipitating cumulus towers. *Monthly Weather Review*, 97(7), 471–489.
- Slingo, J., Blackburn, M., Betts, A., Brugge, R., Hodges, K., Hoskins, B., Miller, M., Steenman-Clark, L. and Thuburn, J. (1994) Mean climate and transience in the tropics of the UGAMP GCM: sensitivity to convective parametrization. *Quarterly Journal of the Royal Meteorological Society*, 120 (518), 881–922.
- Smith, R.K. (2000) The role of cumulus convection in hurricanes and its representation in hurricane models. *Reviews of Geophysics*, 38(4), 465–489.
- Strachan, J., Vidale, P.L., Hodges, K., Roberts, M. and Demory, M.-E. (2013) Investigating global tropical cyclone activity with a hierarchy of AGCMs: the role of model resolution. *Journal of Climate*, 26(1), 133–152.
- Suarez, M.J., Rienecker, M., Todling, R., Bacmeister, J., Takacs, L., Liu, H., Gu, W., Sienkiewicz, M., Koster, R., and Gelaro, R. (2008) *The GEOS-5 Data Assimilation System --Documentation of versions 5.0.1, 5.1.0, and 5.2.0*. NASA Tech. Memo., NASA/TM-2008-104606, 27, 97.
- Tokioka, T., Yamazaki, K., Kitoh, A. and Ose, T. (1988) The equatorial 30–60 day oscillation and the Arakawa-Schubert penetrative cumulus parameterization. *Journal of the Meteorological Society of Japan, Series II*, 66(6), 883–901.
- Vimont, D.J. and Kossin, J.P. (2007) The Atlantic meridional mode and hurricane activity. *Geophysical Research Letters*, 34(7), L07709.
- Vitart, F. and Anderson, J. (2001) Sensitivity of Atlantic tropical storm frequency to ENSO and interdecadal variability of SSTs in an ensemble of AGCM integrations. *Journal of Climate*, 14(4), 533–545.
- Vitart, F., Anderson, J. and Stern, W. (1997) Simulation of interannual variability of tropical storm frequency in an ensemble of GCM integrations. *Journal of Climate*, 10(4), 745–760.
- Waliser, D.E., Lau, K. and Kim, J.-H. (1999) The influence of coupled sea surface temperatures on the Madden-Julian Oscillation: a model perturbation experiment. *Journal of the Atmospheric Sciences*, 56(3), 333–358.
- Walsh, K., Fiorino, M., Landsea, C. and McInnes, K. (2007) Objectively determined resolution-dependent threshold criteria for the detection of tropical cyclones in climate models and reanalyses. *Journal of Climate*, 20(10), 2307–2314.
- Walsh, K., Lavender, S., Scoccimarro, E. and Murakami, H. (2013) Resolution dependence of tropical cyclone formation in CMIP3 and finer resolution models. *Climate Dynamics*, 40(3–4), 585–599.
- Walsh, K.J., Camargo, S.J., Vecchi, G.A., Daloz, A.S., Elsner, J., Emanuel, K., Horn, M., Lim, Y.-K., Roberts, M. and Patricola, C. (2015) Hurricanes and climate: the US CLIVAR working group on hurricanes. *Bulletin of the American Meteorological Society*, 96(6), 997–1017.
- Wang, C., Lee, S.K. and Enfield, D.B. (2008) Atlantic warm pool acting as a link between Atlantic Multidecadal Oscillation and Atlantic tropical cyclone activity. *Geochemistry, Geophysics, Geosystems*, 9(5), Q05V03.
- Wang, H., Long, L., Kumar, A., Wang, W., Schemm, J.-K.E., Zhao, M., Vecchi, G.A., Larow, T.E., Lim, Y.-K. and Schubert, S.D. (2014) How well do global climate models simulate the variability of Atlantic tropical cyclones associated with ENSO? *Journal of Climate*, 27(15), 5673–5692.
- Yoo, C., Park, S., Kim, D., Yoon, J.-H. and Kim, H.-M. (2015) Boreal winter MJO teleconnection in the Community Atmosphere Model version 5 with the unified convection parameterization. *Journal of Climate*, 28(20), 8135–8150.
- Zhang, W., Vecchi, G.A., Murakami, H., Delworth, T., Wittenberg, A.T., Rosati, A., Underwood, S., Anderson, W., Harris, L. and Gudgel, R. (2016) Improved simulation of tropical cyclone responses to ENSO in the western North Pacific in the high-resolution GFDL HiFLOR coupled climate model. *Journal of Climate*, 29(4), 1391–1415.
- Zhao, M., Held, I.M. and Lin, S.-J. (2012) Some counterintuitive dependencies of tropical cyclone frequency on parameters in a GCM. *Journal of the Atmospheric Sciences*, 69(7), 2272–2283.
- Zhao, M., Held, I.M., Lin, S.-J. and Vecchi, G.A. (2009) Simulations of global hurricane climatology, interannual variability, and response to global warming using a 50-km resolution GCM. *Journal of Climate*, 22(24), 6653–6678.

SUPPORTING INFORMATION

Additional supporting information may be found online in the Supporting Information section at the end of this article.

How to cite this article: Seo E, Lee M-I, Kim D, Lim Y-K, Schubert SD, Kim K-M. Inter-annual variation of tropical cyclones simulated by GEOS-5 AGCM with modified convection scheme. *Int J Climatol*. 2019;1–17. <https://doi.org/10.1002/joc.6058>